Supplementary data for article :

Pavic, A.; Glišić, B. Đ.; Vojnovic, S.; Warżajtis, B.; Savić, N. D.; Antić, M.; Radenković, S.; Janjić, G. V.; Nikodinovic-Runic, J.; Rychlewska, U.; et al. Mononuclear Gold(III) Complexes with Phenanthroline Ligands as Efficient Inhibitors of Angiogenesis: A Comparative Study with Auranofin and Sunitinib. *Journal of Inorganic Biochemistry* **2017**, *174*, 156–168. https://doi.org/10.1016/j.jinorgbio.2017.06.009

Ms. No. JINORGBIO_2017_213 (revised version)

Mononuclear gold(III) complexes with phenanthroline ligands as efficient inhibitors of angiogenesis: a comparative study with auranofin and sunitinib

Aleksandar Pavic[a,*], Biljana Đ. Glišić[b,*], Sandra Vojnovic[a], Beata Warżajtis[c], Nada D. Savić[b], Marija Antić[b], Slavko Radenković[b], Goran V. Janjić[d], Jasmina Nikodinovic-Runic[a], Urszula Rychlewska[c], Miloš I. Djuran[b,e]

[a]*Institute of Molecular Genetics and Genetic Engineering, University of Belgrade, Vojvode Stepe 444a, 11000 Belgrade, Serbia*

[b]*University of Kragujevac, Faculty of Science, Department of Chemistry, R. Domanovića 12, PO Box 60, 34000 Kragujevac, Serbia*

[c]*Faculty of Chemistry, Adam Mickiewicz University, Umultowska 89B, 61-614 Poznań, Poland*

[d]*Institute of Chemistry, Metallurgy and Technology, University of Belgrade, Njegoševa 12, 11000 Belgrade, Serbia*

[e]*Serbian Academy of Sciences and Arts, Knez Mihailova 35, 11000 Belgrade, Serbia*

[*]Corresponding authors: Tel.: +381 11 397 6034; fax: +381 11 397 5808 (A. Pavic); Tel.: +381 34 300 251; fax: +381 34 335 040 (B. Đ. Glišić).

E-mail addresses: sasapavic@imgge.bg.ac.rs (A. Pavic); bglisic@kg.ac.rs (B. Đ. Glišić).

Abstract

Gold(III) complexes with 1,7- and 4,7-phenanthroline ligands, [$AuCl_3$(1,7-phen-κ*N*7)] (**1**) and [$AuCl_3$(4,7-phen-κ*N*4)] (**2**) were synthesized and structurally characterized by spectroscopic (NMR, IR and UV-vis) and single-crystal X-ray diffraction techniques. In these complexes, 1,7- and 4,7-phenanthrolines are monodentatedly coordinated to the Au(III) ion through the N7 and N4 nitrogen atoms, respectively. In comparison to the clinically relevant anti-angiogenic compounds auranofin and sunitinib, gold(III)-phenanthroline complexes showed from 1.5- to 20-fold higher anti-angiogenic potential, and 13- and 118-fold lower toxicity. Among the tested compounds, complex **1** was the most potent and may be an excellent anti-angiogenic drug candidate, since it showed strong anti-angiogenic activity in zebrafish embryos achieving IC_{50} value (concentration resulting in an anti-angiogenic phenotype at 50% of embryos) of 2.89 μM, while had low toxicity with LC_{50} value (the concentration inducing the lethal effect of 50% embryos) of 128 μM. Molecular docking study revealed that both complexes and ligands could suppress angiogenesis targeting the multiple major regulators of angiogenesis, such as the vascular endothelial growth factor receptor (VEGFR-2), the matrix metalloproteases (MMP-2 and MMP-9), and thioredoxin reductase (TrxR1), where the complexes showed higher binding affinity in comparison to ligands, and particularly to auranofin, but comparable to sunitinib, an anti-angiogenic drug of clinical relevance.

Keywords: Gold(III) complexes, Phenanthroline, Cytotoxicity, Embryotoxicity, Angiogenesis

TABLE OF CONTENTS

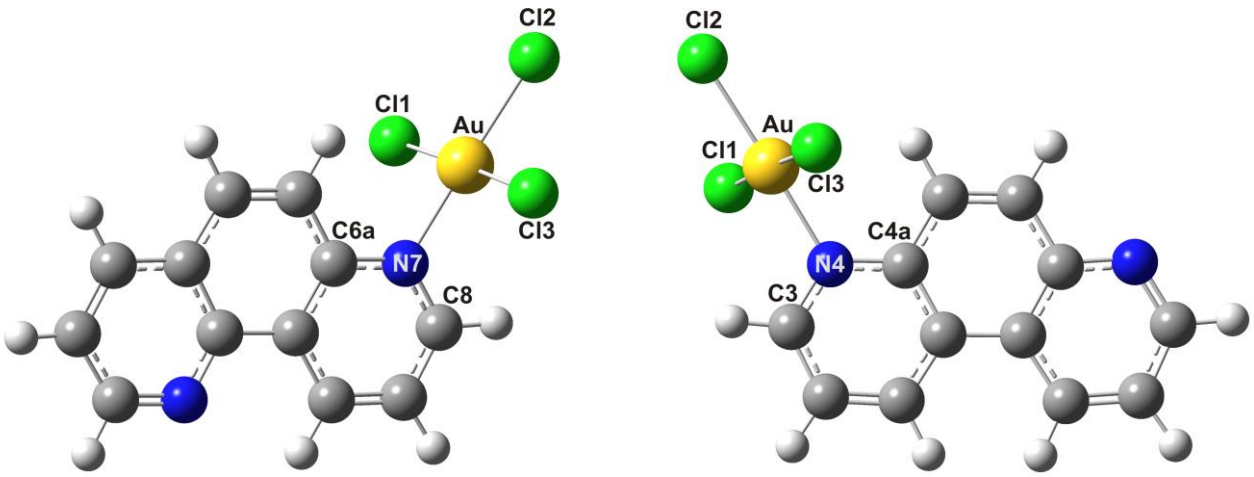

[$AuCl_3$(1,7-phen-κ*N*7)] (**1**) [$AuCl_3$(4,7-phen-κ*N*4)] (**2**)

Fig. S1. The structures of mononuclear gold(III) complexes **1** and **2** calculated at the M06-2X(CPCM)/cc-pVTZ+LanL2TZ(f) level of theory.

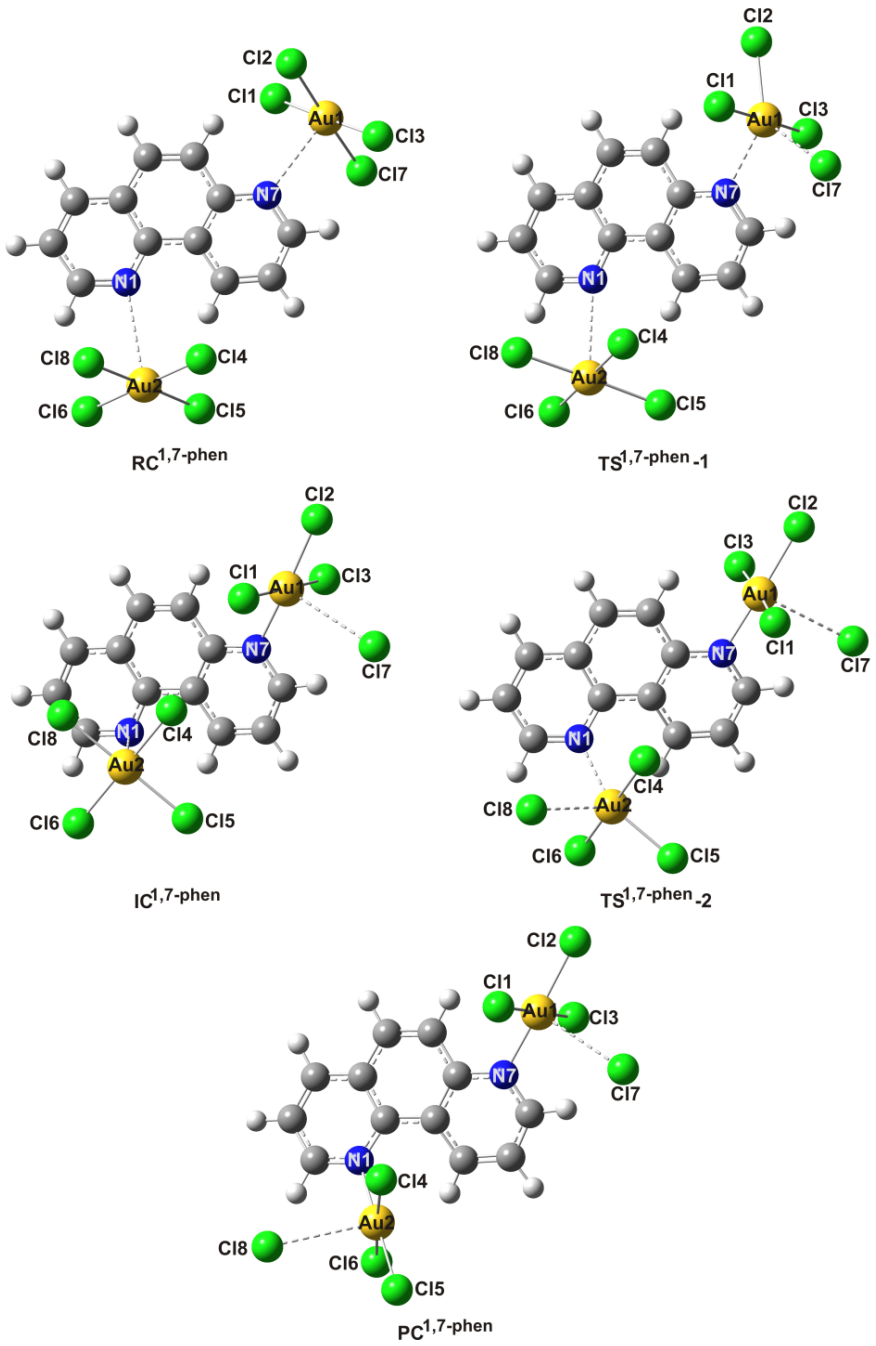

Fig. S2. Optimized geometries of the chemical species involved in the reaction of $[AuCl_4]^-$ with 1,7-phen in 2 : 1 molar ratio, respectively, calculated at the M06-2X(CPCM)/cc-pVTZ+LanL2TZ(f) level of theory. The reaction pathway is the following: $RC^{1,7\text{-phen}}$ (reactant complex) → $TS^{1,7\text{-phen}}$-1 (transition state 1) → $IC^{1,7\text{-phen}}$ (intermediate complex) → $TS^{1,7\text{-phen}}$-2 (transition state 2) → $PC^{1,7\text{-phen}}$ (product complex).

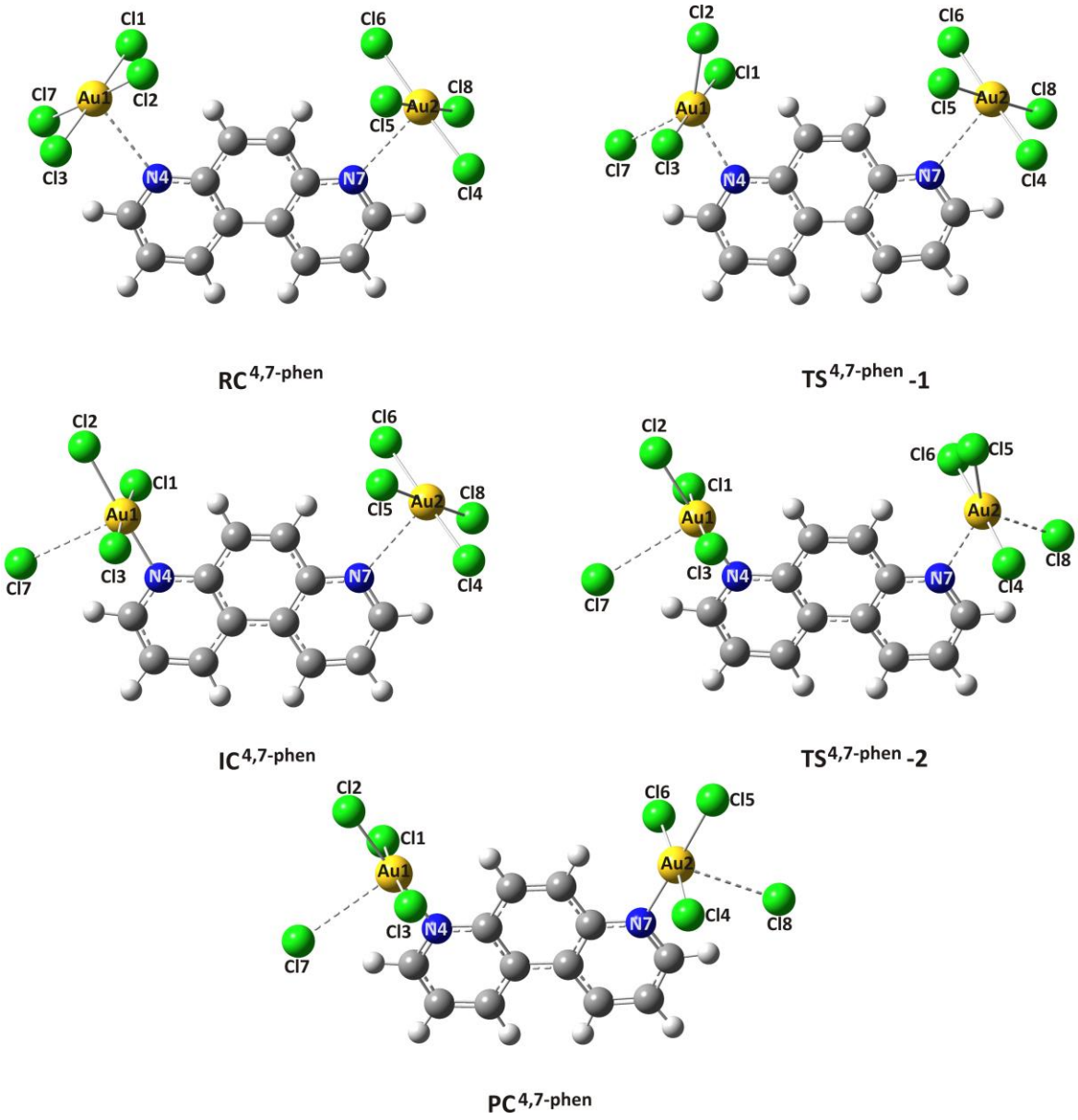

Fig. S3. Optimized geometries of the chemical species involved in the reaction of $[AuCl_4]^-$ with 4,7-phen in 2 : 1 molar ratio, respectively, calculated at the M06-2X(CPCM)/cc-pVTZ+LanL2TZ(f) level of theory. The reaction pathway is the following: $RC^{4,7\text{-phen}}$ (reactant complex) → $TS^{4,7\text{-phen}}$-1 (transition state 1) → $IC^{4,7\text{-phen}}$ (intermediate complex) → $TS^{4,7\text{-phen}}$-2 (transition state 2) → $PC^{4,7\text{-phen}}$ (product complex).

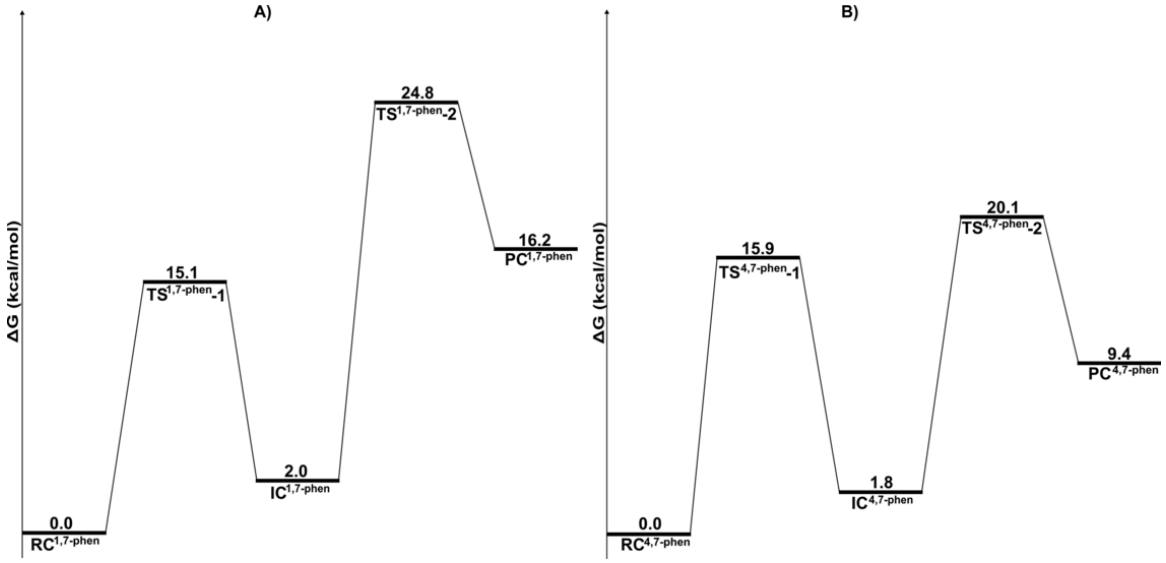

Fig. S4. Energy diagram of the reactions of $[AuCl_4]^-$ with 1,7-phen (A) and 4,7-phen (B) in 2 : 1 molar ratio, respectively. Relative free energies (M06-2X(CPCM)/cc-pVTZ+LanL2TZ(f)) were computed with respect to the corresponding reactant complex. For more details see Figs. S2 and S3.

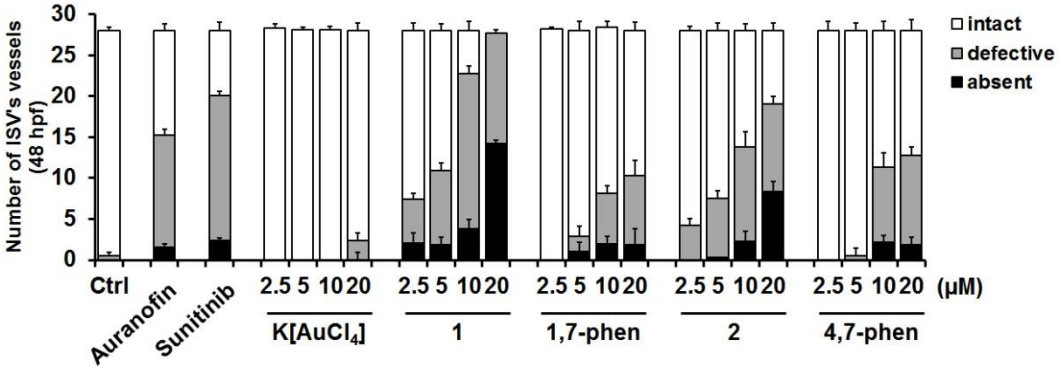

Fig. S5. The anti-angiogenic phenotype of zebrafish embryos defined as effect of different concentrations of gold(III)-phenanthroline complexes **1** and **2**, the respective 1,7-and 4,7-phen ligands and $K[AuCl_4]$ on the ISVs development. 1.25 μM auranofin and sunitinib were used as positive controls.

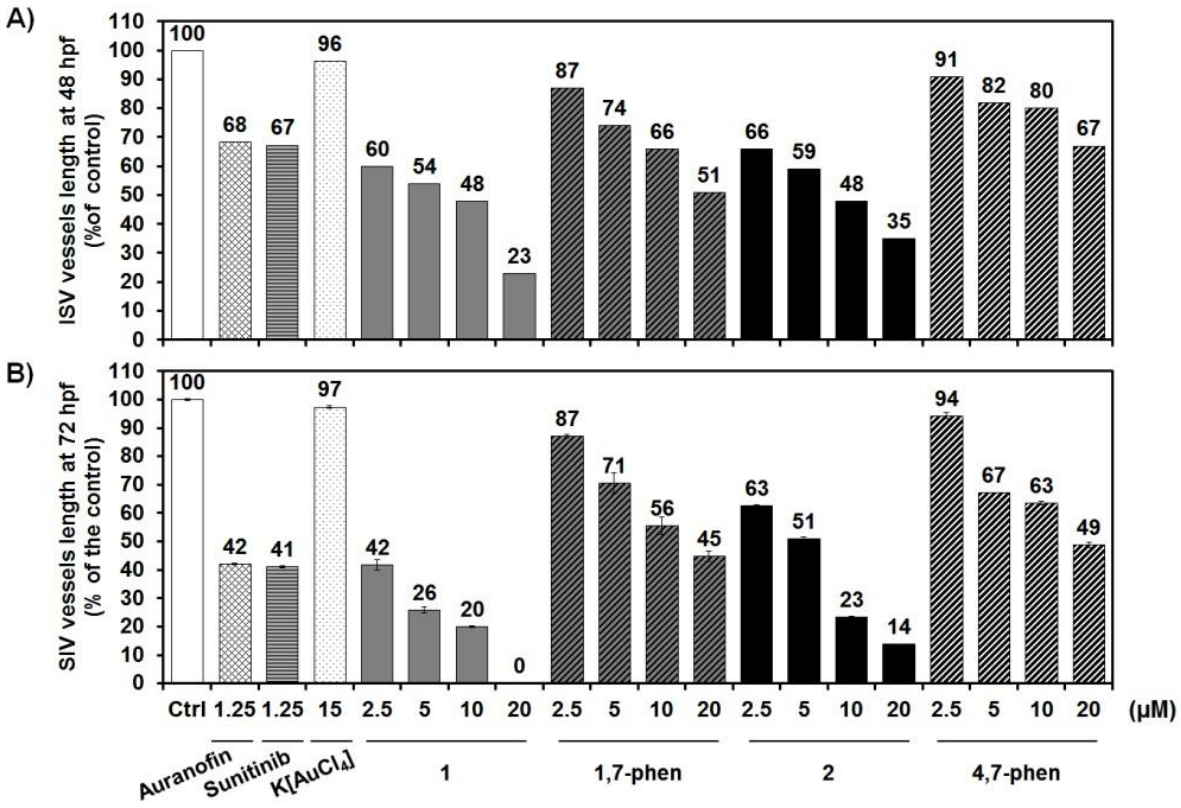

Fig. S6. The inhibition of ISVs and SIVs angiogenesis upon treatments with different concentrations of gold(III)-phenanthroline complexes **1** and **2**, the respective 1,7- and 4,7-phen ligands and $K[AuCl_4]$ on the ISVs development. 1.25 μM auranofin and sunitinib were used as positive controls.

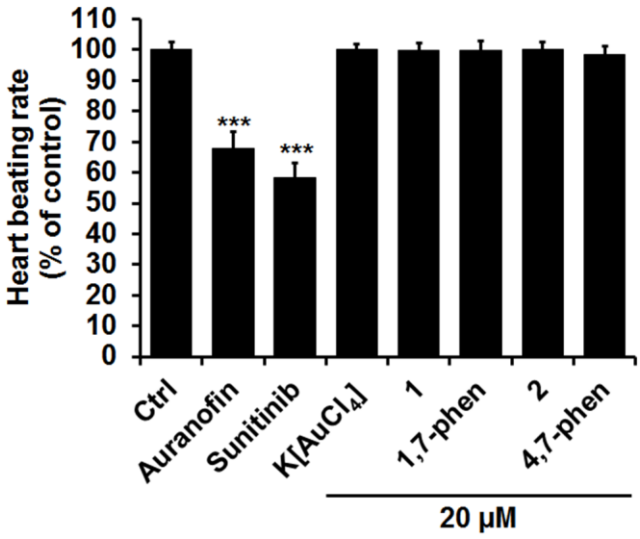

Fig. S7. The effect of different concentrations of gold(III)-phenanthroline complexes **1** and **2**, the respective 1,7- and 4,7-phen ligands and $K[AuCl_4]$ on the heart beating rate of zebrafish embryos (n = 30). Auranofin and sunitinib applied in the concentration of 1.25 µM were used as positive controls.

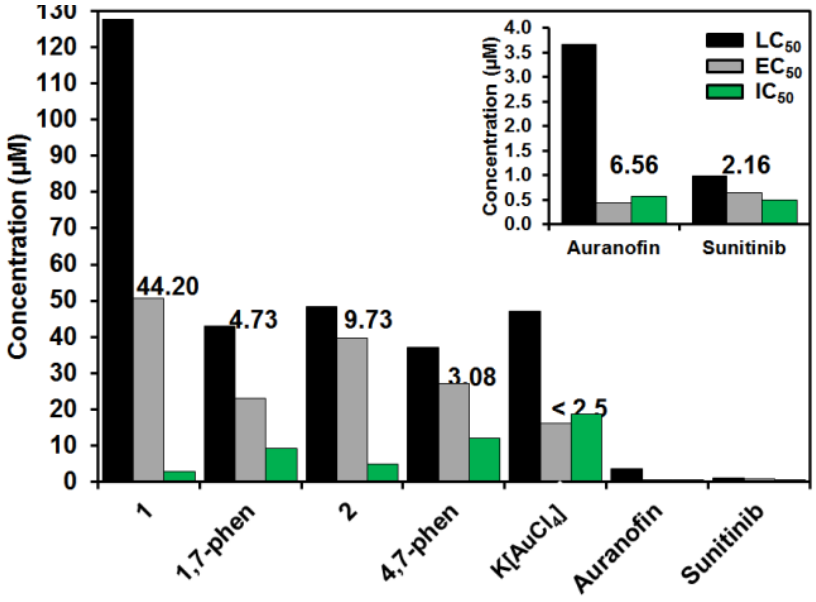

Fig. S8. Therapeutic window (TW) of gold(III)-phenanthroline complexes **1** and **2**, the respective 1,7- and 4,7-phen ligands, $K[AuCl_4]$, auranofin and sunitinib assessed as the ratio of LC_{50} and IC_{50}. Respective TW values are presented above each of tested compounds.

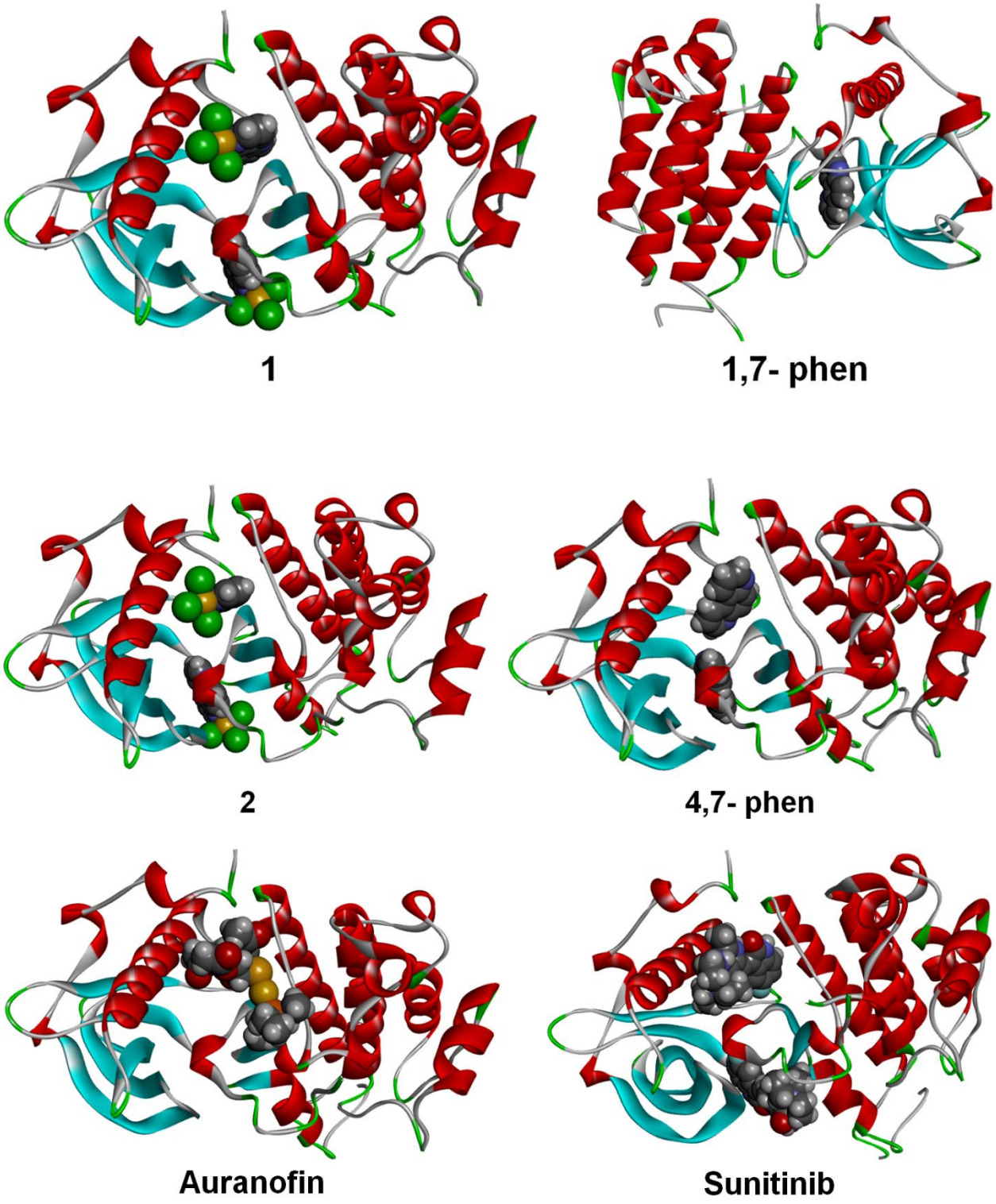

Fig. S9. The binding of gold(III) complexes **1** and **2**, 1,7- and 4,7-phen, auranofin and sunitinib in the active site of VEGFR-2 protein as assessed by molecular docking.

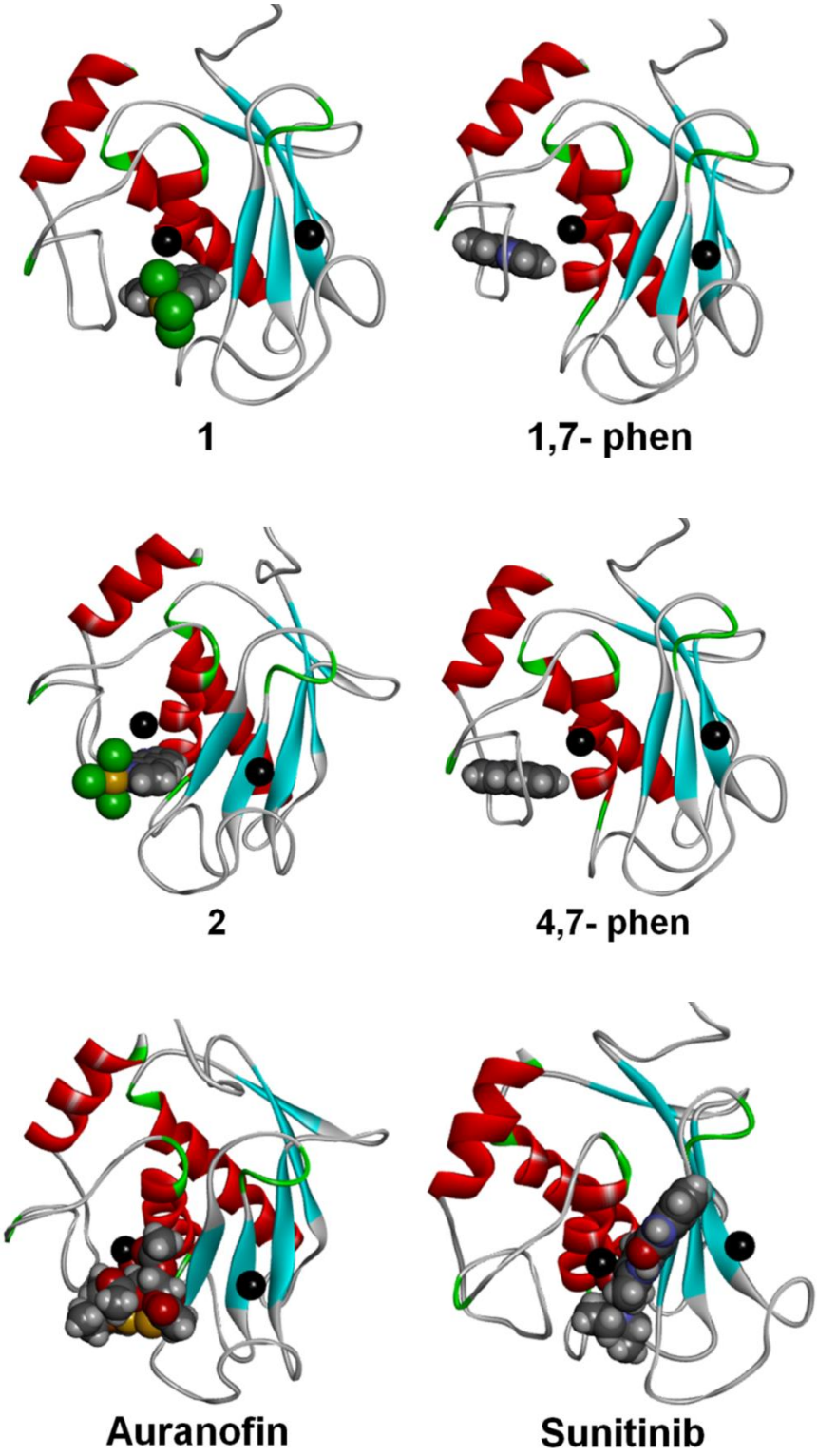

Fig. S10. The binding of gold(III) complexes **1** and **2**, 1,7- and 4,7-phen, auranofin and sunitinib in the active site of MMP-2 protein as assessed by molecular docking.

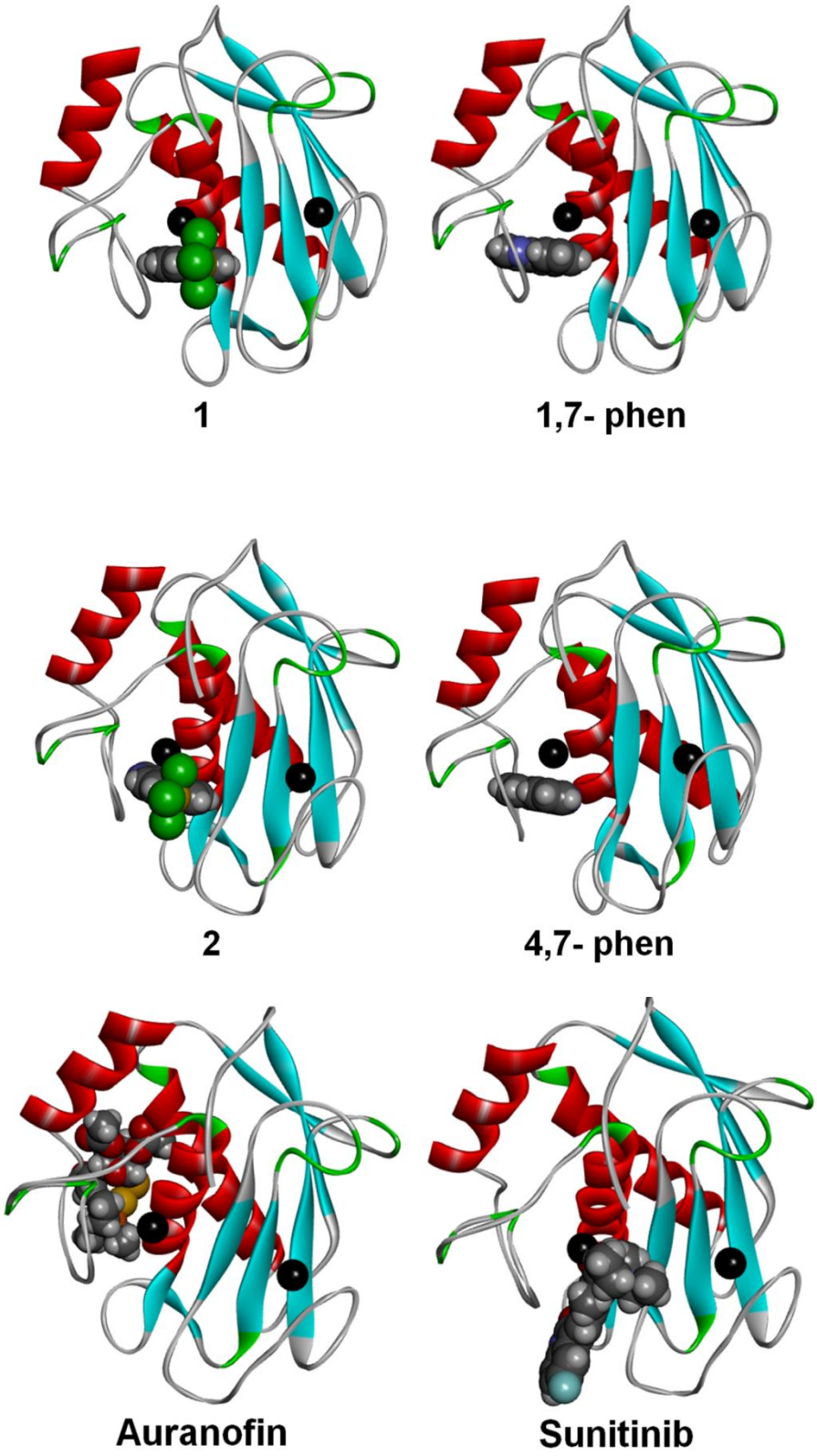

Fig. S11. The binding of gold(III) complexes **1** and **2**, 1,7- and 4,7-phen, auranofin and sunitinib in the active site of MMP-9 protein as assessed by molecular docking.

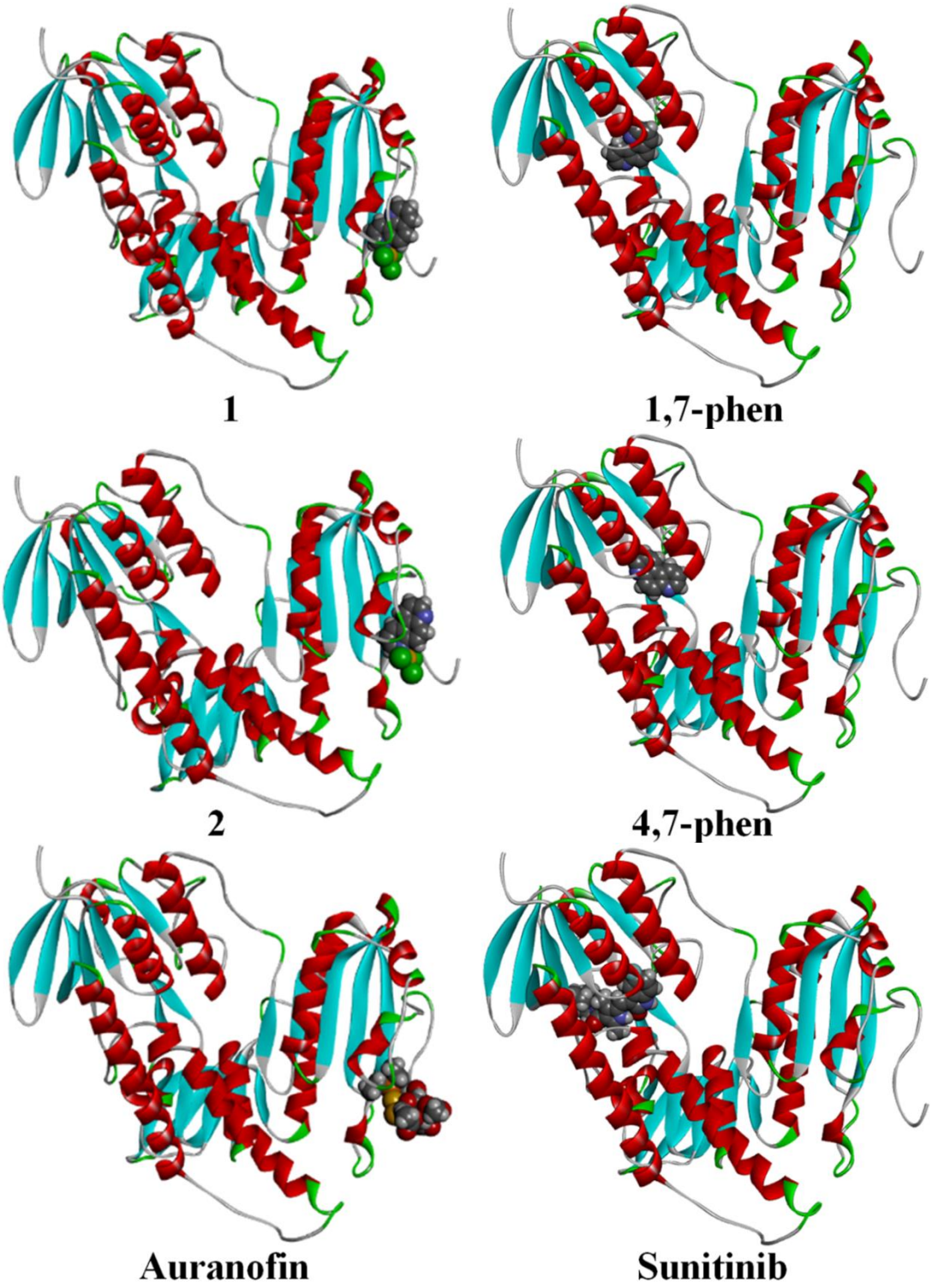

Fig. S12. The binding of gold(III) complexes **1** and **2**, 1,7- and 4,7-phen, auranofin and sunitinib in the active site of the protein thioredoxin reductase 1 (TrxR1) as assessed by molecular docking.

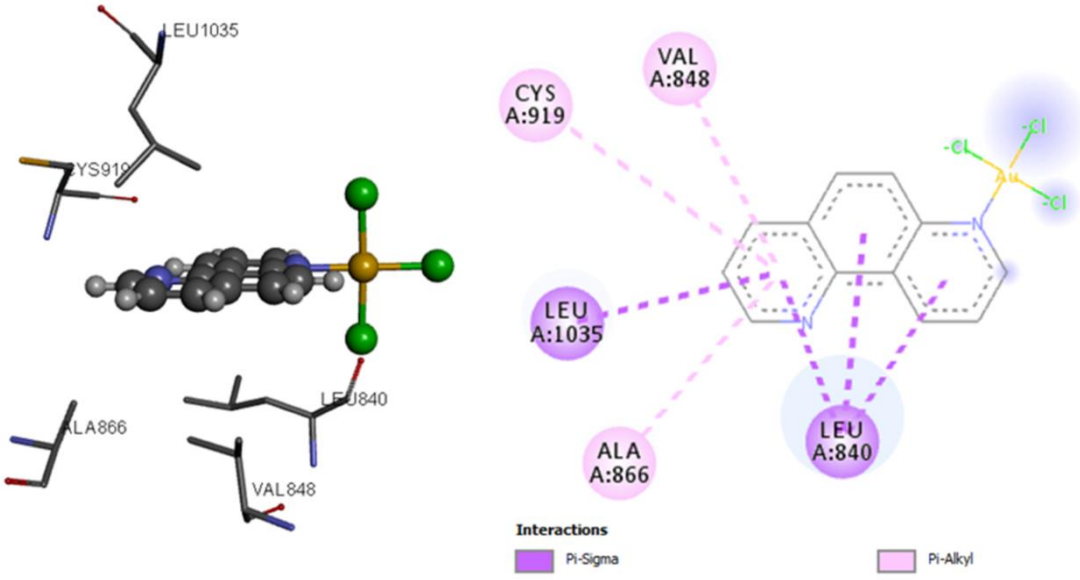
LEU1035
CYS919
LEU840
ALA866
VAL848
CYS A:919
VAL A:848
LEU A:1035
ALA A:866
LEU A:840
Cl
Cl
Cl
Au
N
N
Interactions
Pi-Sigma
Pi-Alkyl

1

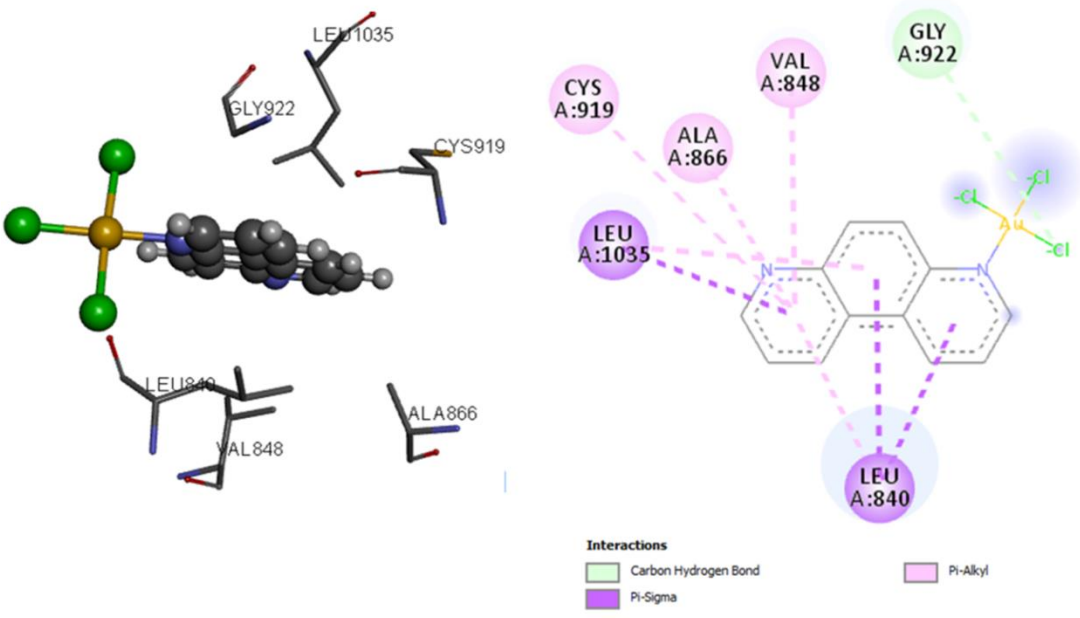
LEU1035
GLY922
CYS919
LEU840
ALA866
VAL848
GLY A:922
VAL A:848
CYS A:919
ALA A:866
LEU A:1035
LEU A:840
Cl
Cl
Cl
Au
N
N
Interactions
Carbon Hydrogen Bond
Pi-Alkyl
Pi-Sigma

2

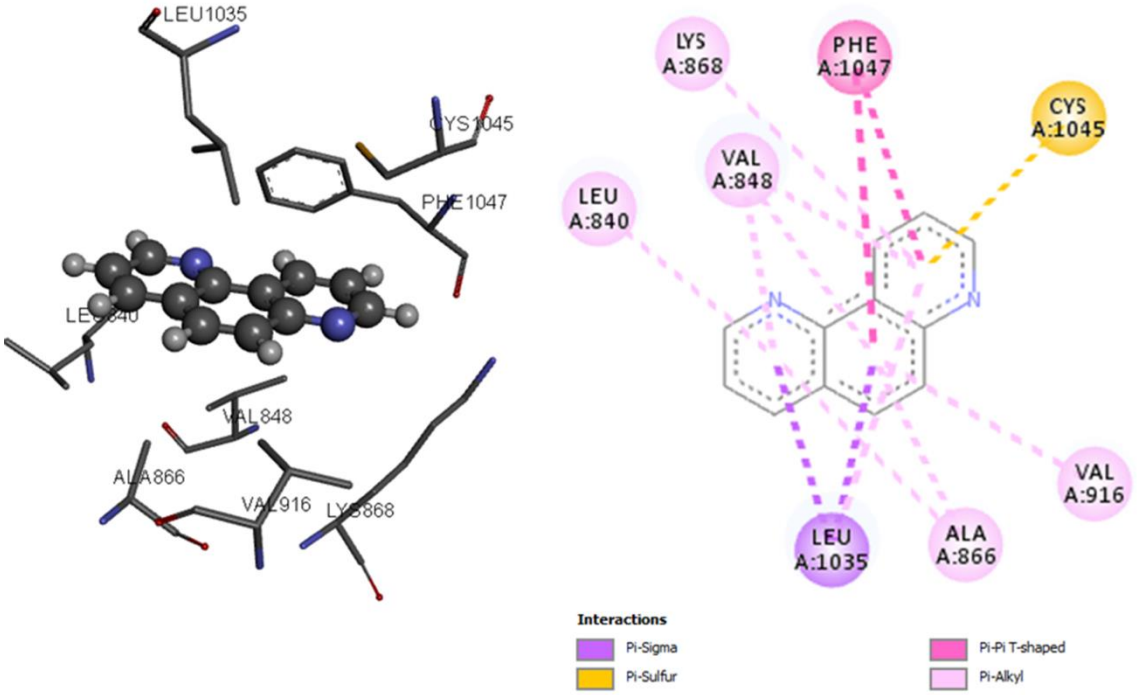

1,7- phen

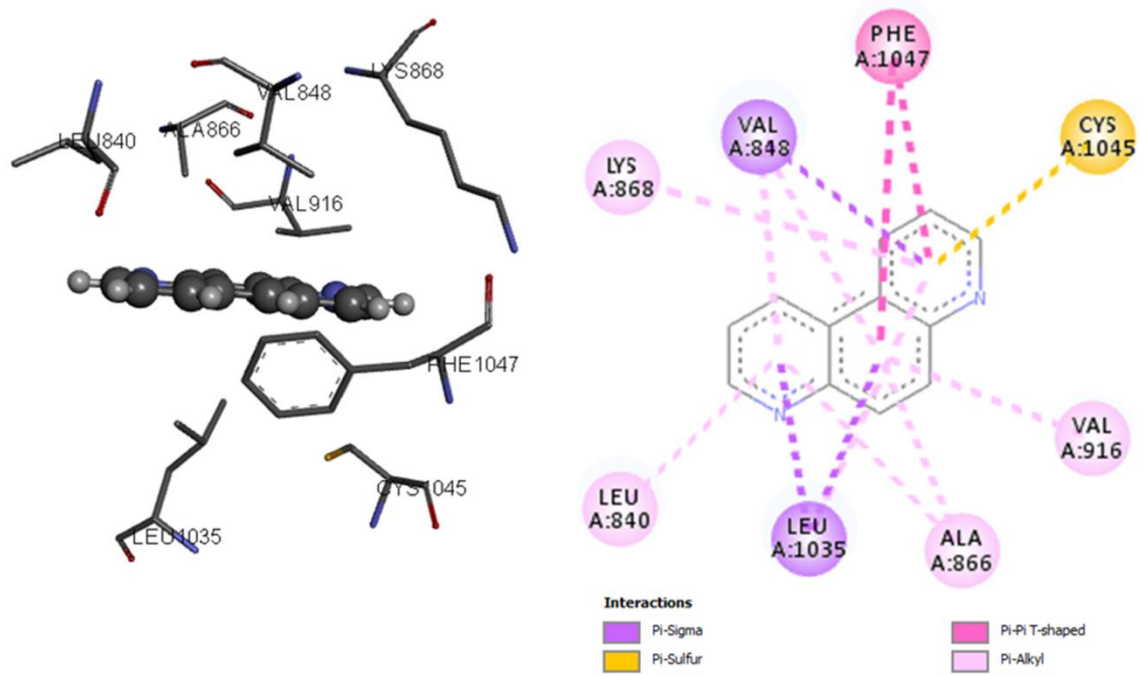

4,7- phen

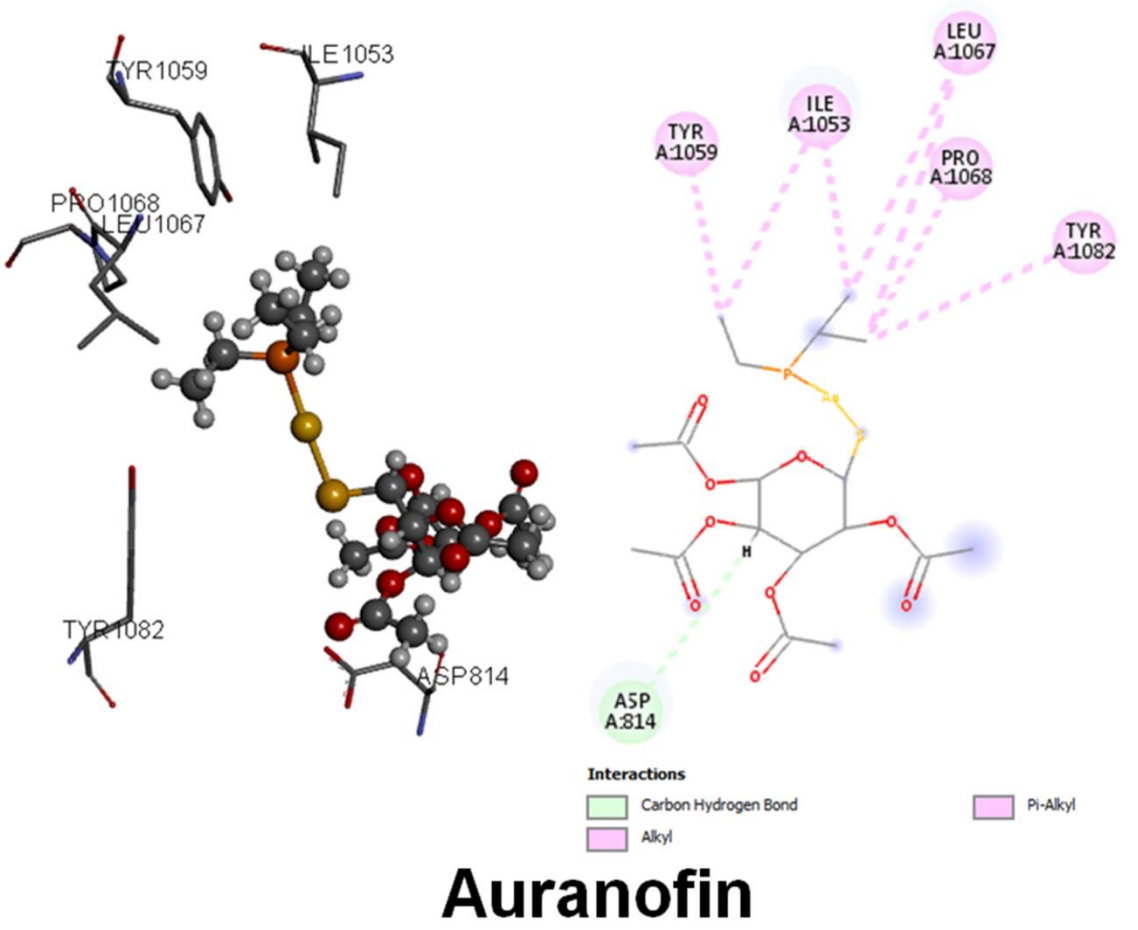

Auranofin

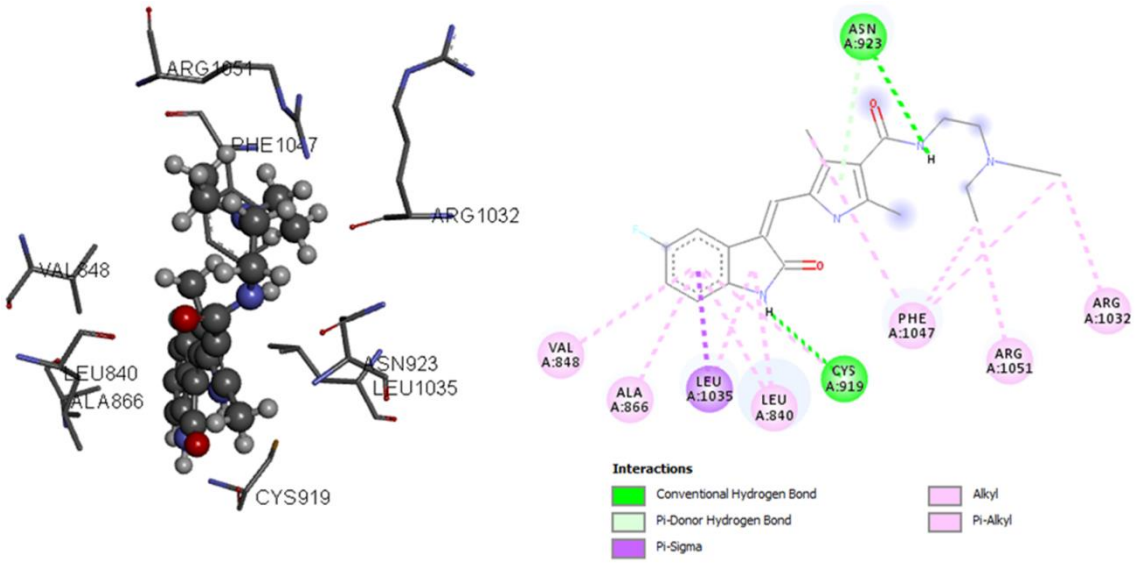

Sunitinib

Fig. S13. Interactions of gold(III) complexes **1** and **2**, 1,7- and 4,7-phen, auranofin and sunitinib with VEGFR-2 protein during molecular docking.

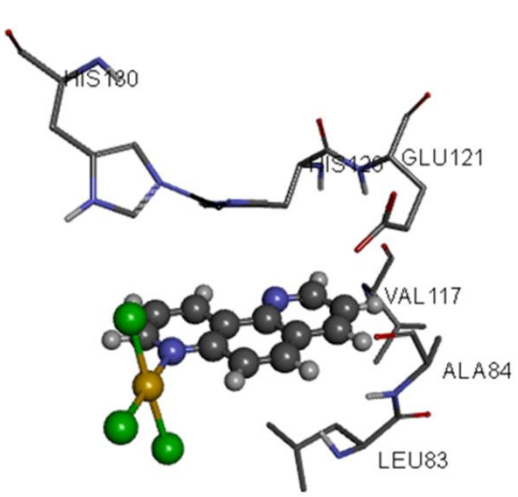
HIS180
GLU121
VAL117
ALA84
LEU83

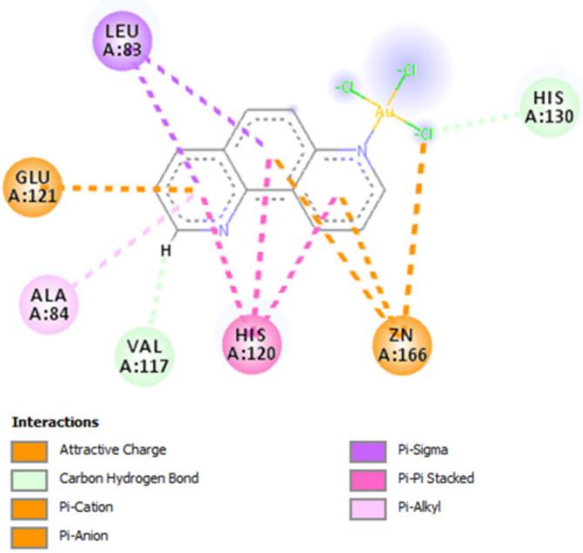
LEU A:83
HIS A:130
GLU A:121
ALA A:84
VAL A:117
HIS A:120
ZN A:166
Interactions
Attractive Charge
Carbon Hydrogen Bond
Pi-Cation
Pi-Anion
Pi-Sigma
Pi-Pi Stacked
Pi-Alkyl

1

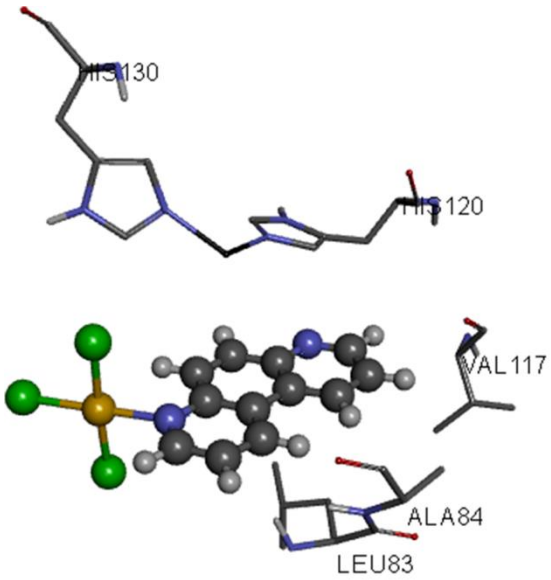
HIS130
HIS120
VAL117
ALA84
LEU83

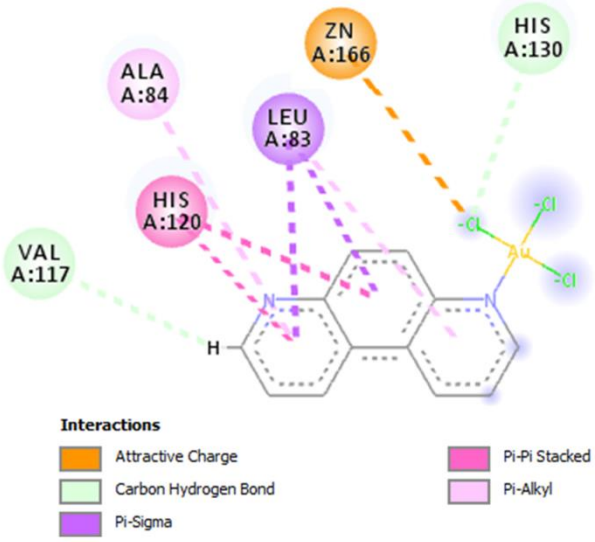
ZN A:166
HIS A:130
ALA A:84
LEU A:83
HIS A:120
VAL A:117
Interactions
Attractive Charge
Carbon Hydrogen Bond
Pi-Sigma
Pi-Pi Stacked
Pi-Alkyl

2

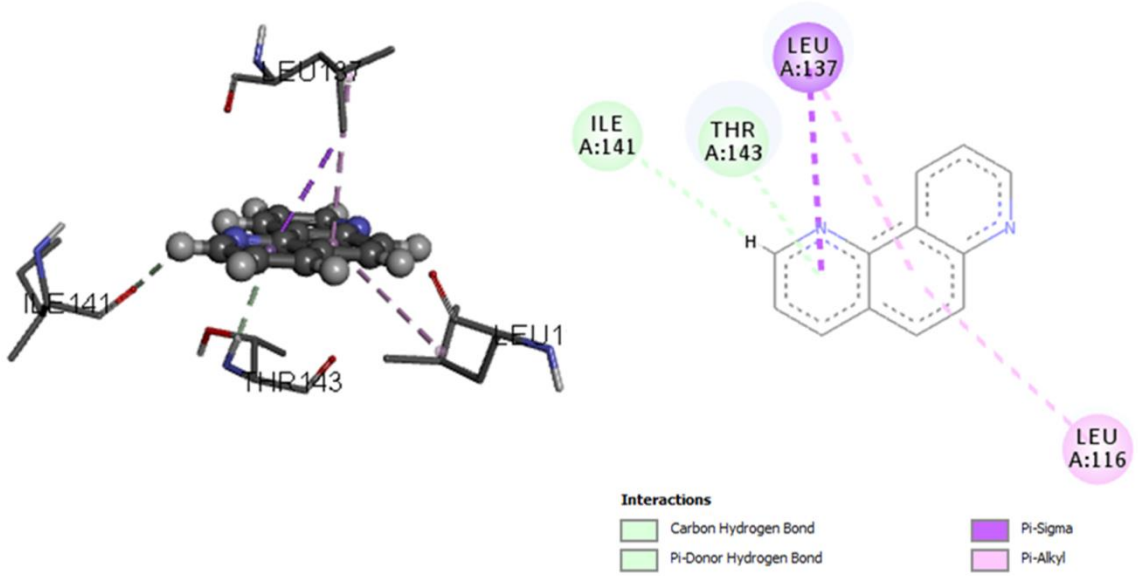

1,7- phen

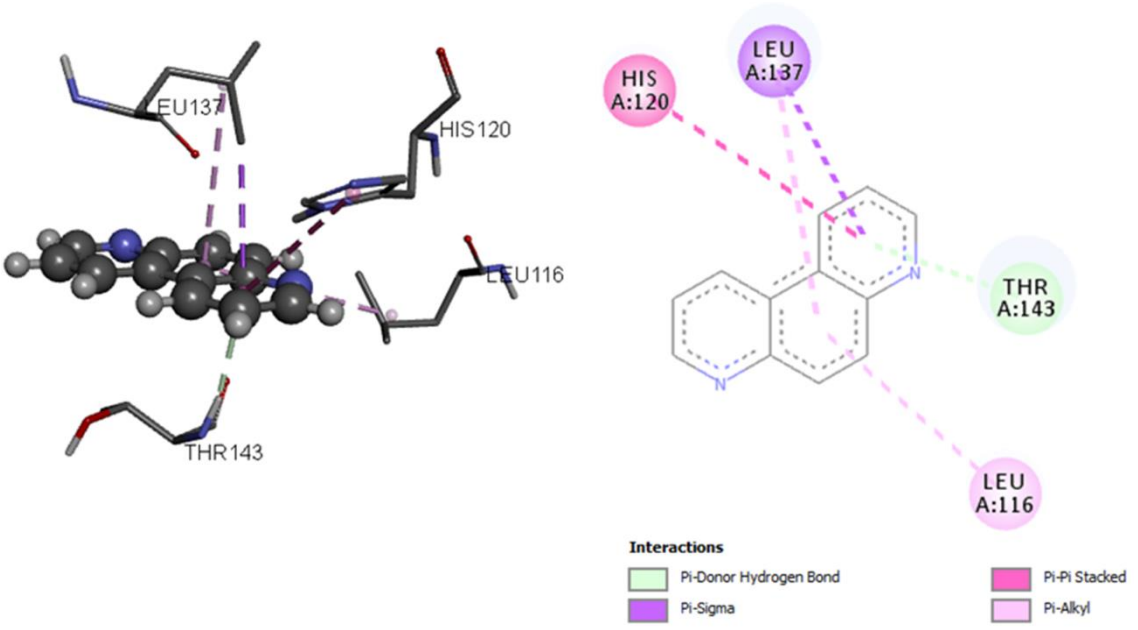

4,7- phen

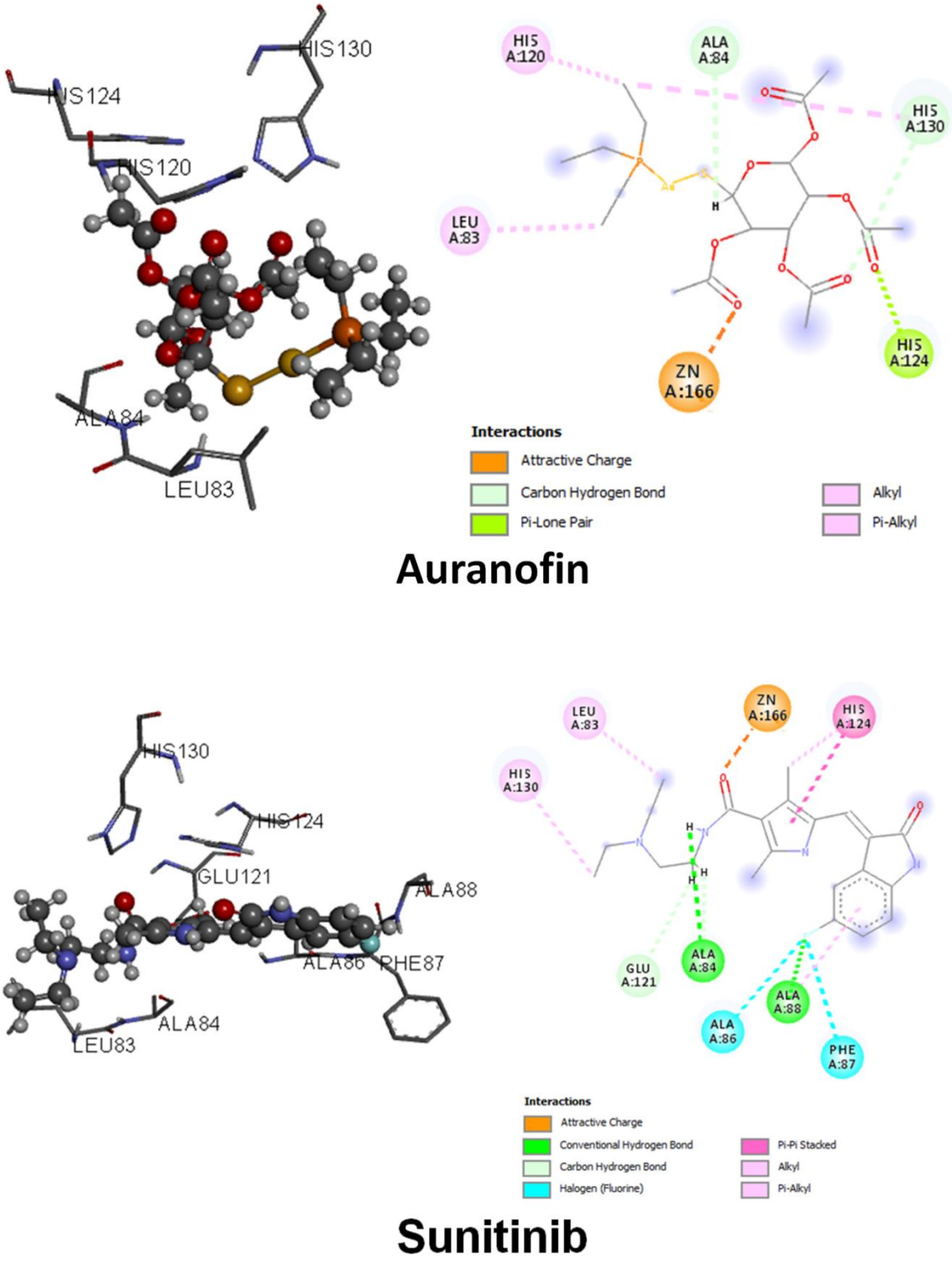

Fig. S14. Interactions of gold(III) complexes **1** and **2**, 1,7- and 4,7-phen, auranofin and sunitinib with MMP-2 protein during molecular docking.

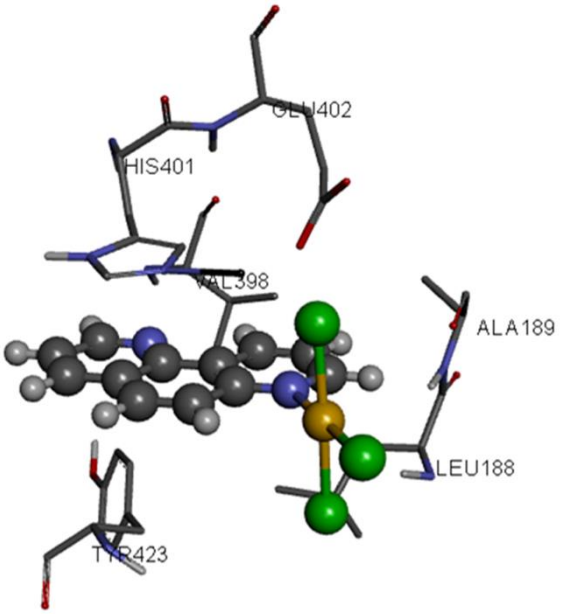
GLU402
HIS401
VAL398
ALA189
LEU188
TYR423

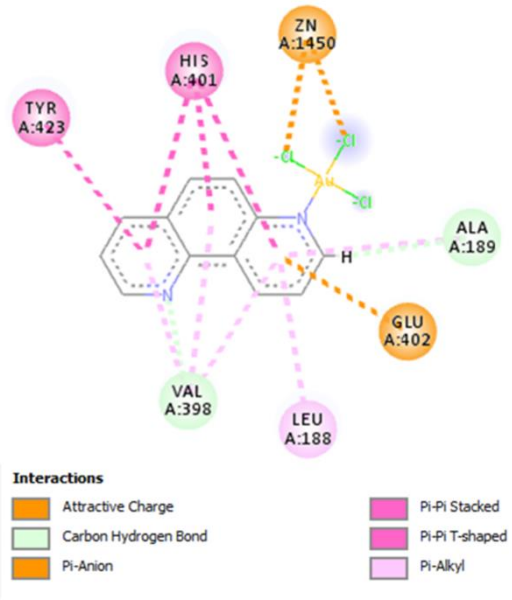
ZN A:1450
HIS A:401
TYR A:423
ALA A:189
GLU A:402
VAL A:398
LEU A:188
Interactions
Attractive Charge
Carbon Hydrogen Bond
Pi-Anion
Pi-Pi Stacked
Pi-Pi T-shaped
Pi-Alkyl

1

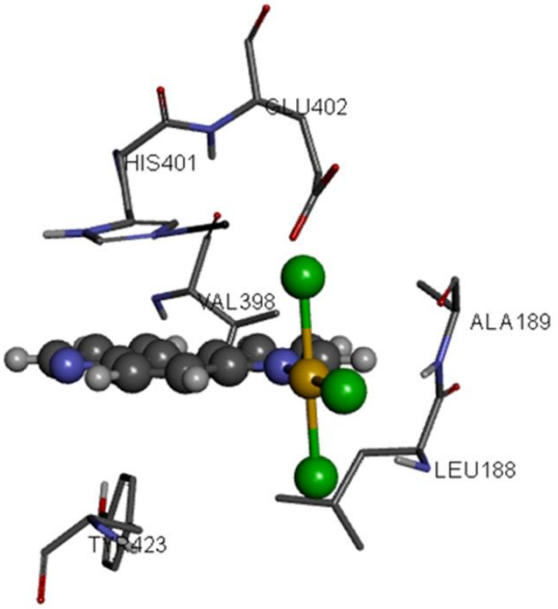
GLU402
HIS401
VAL398
ALA189
LEU188
TYR423

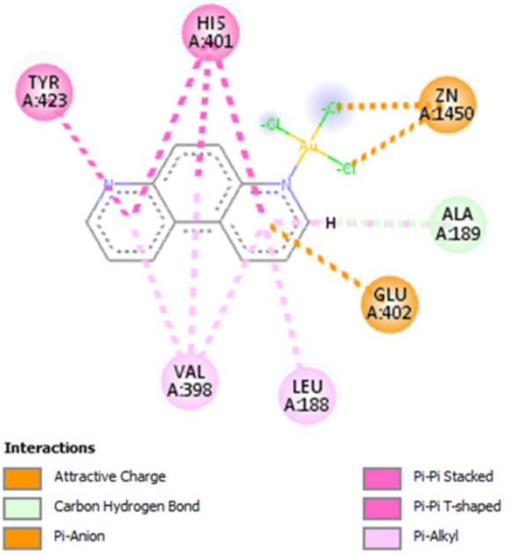
HIS A:401
TYR A:423
ZN A:1450
ALA A:189
GLU A:402
VAL A:398
LEU A:188
Interactions
Attractive Charge
Carbon Hydrogen Bond
Pi-Anion
Pi-Pi Stacked
Pi-Pi T-shaped
Pi-Alkyl

2

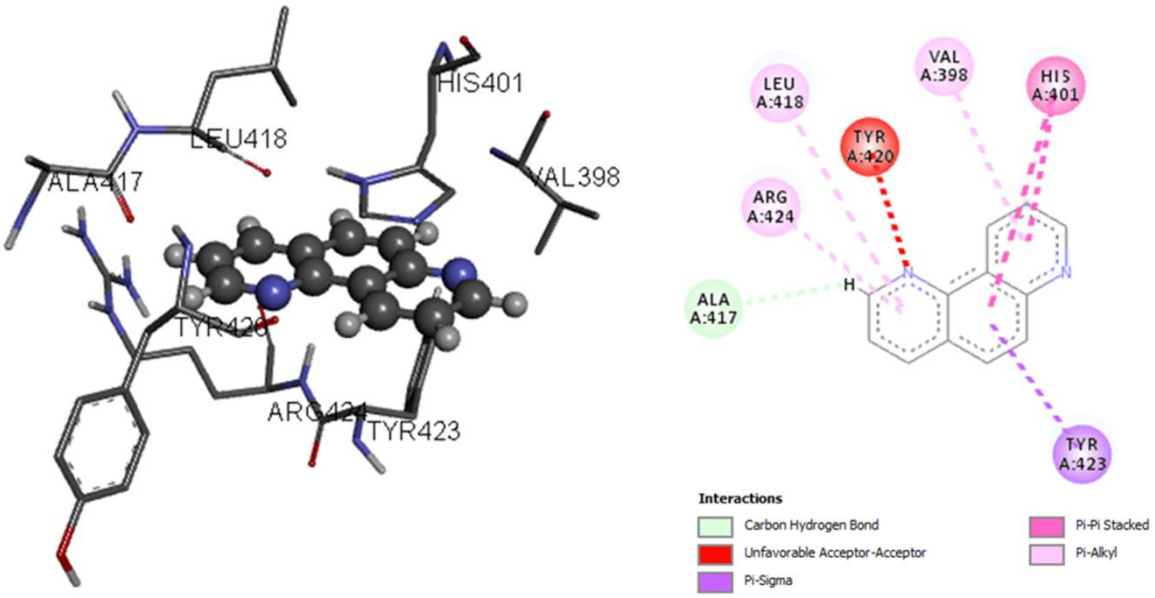

1,7- phen

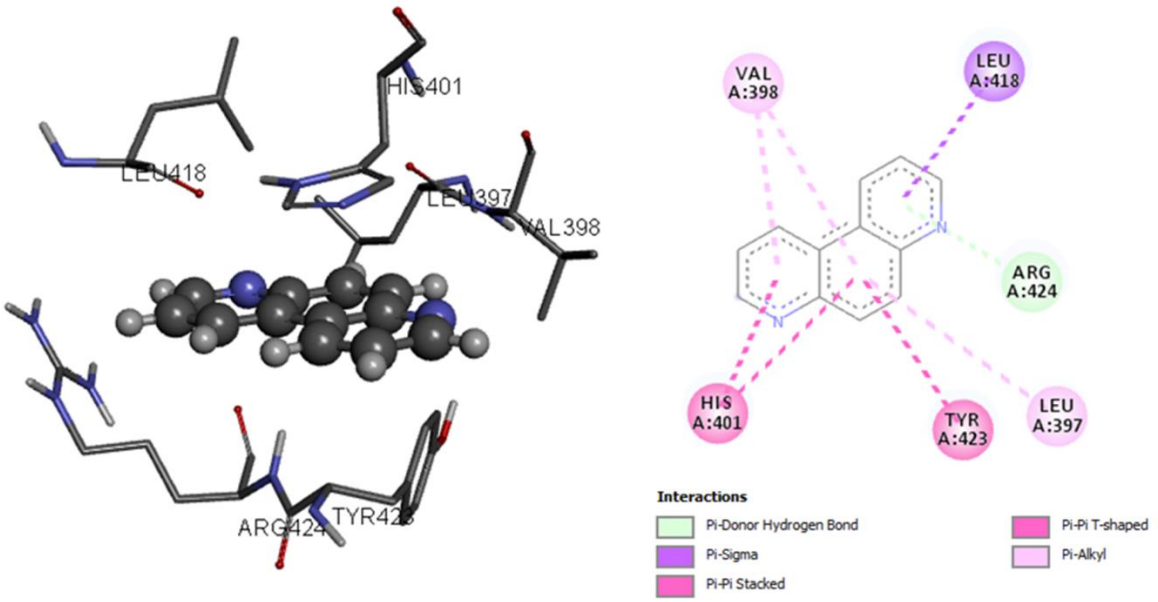

4,7- phen

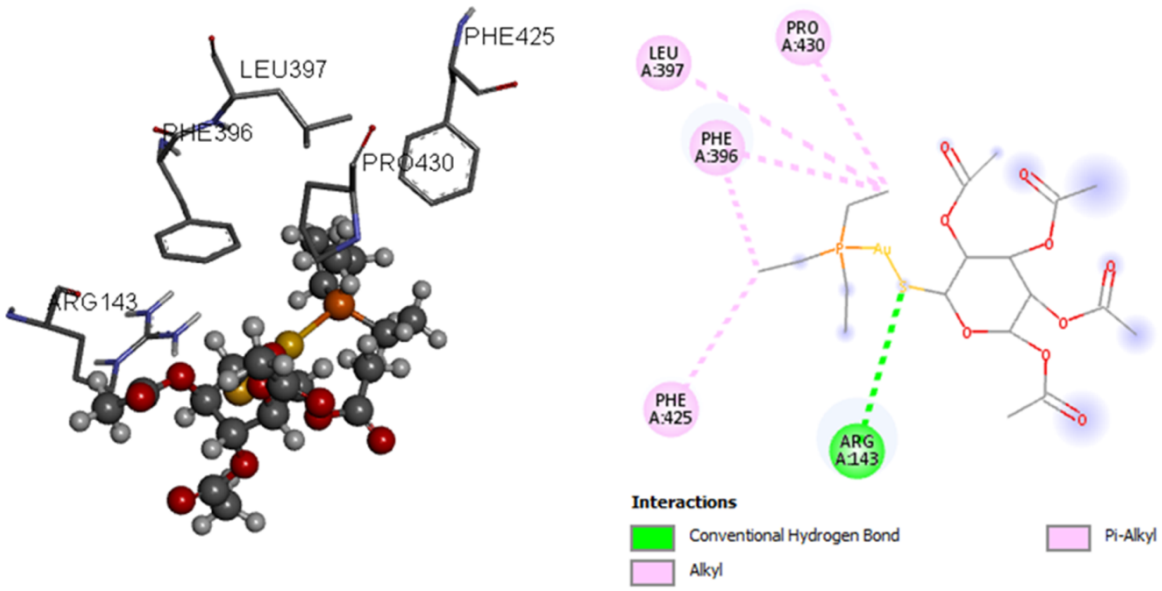

Auranofin

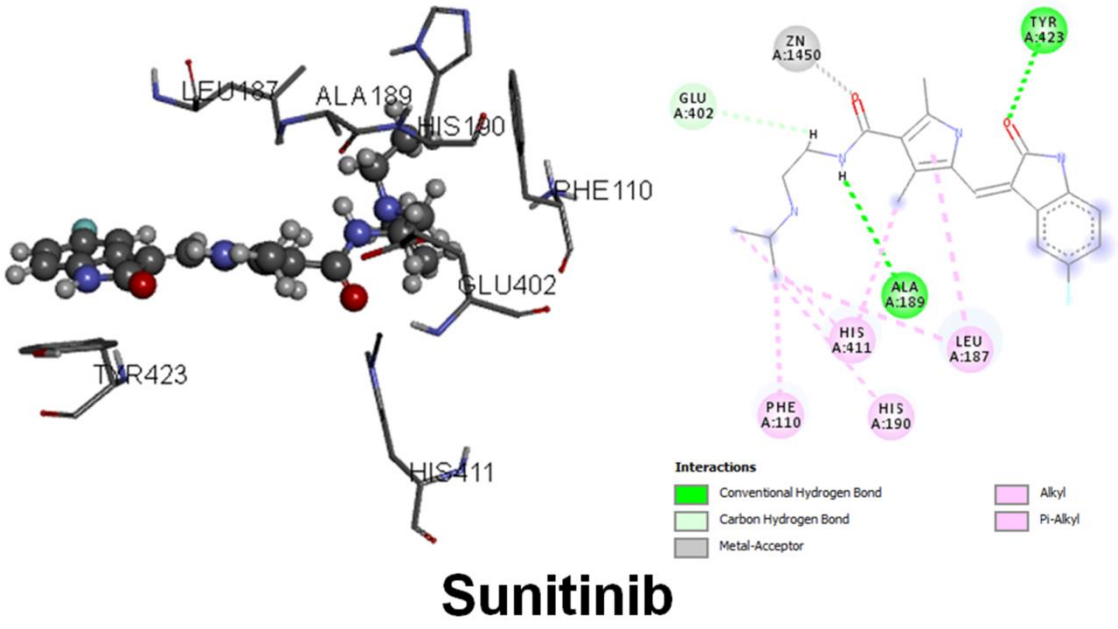

Sunitinib

Fig. S15. Interactions of gold(III) complexes **1** and **2**, 1,7- and 4,7-phen, auranofin and sunitinib with MMP-9 protein during molecular docking.

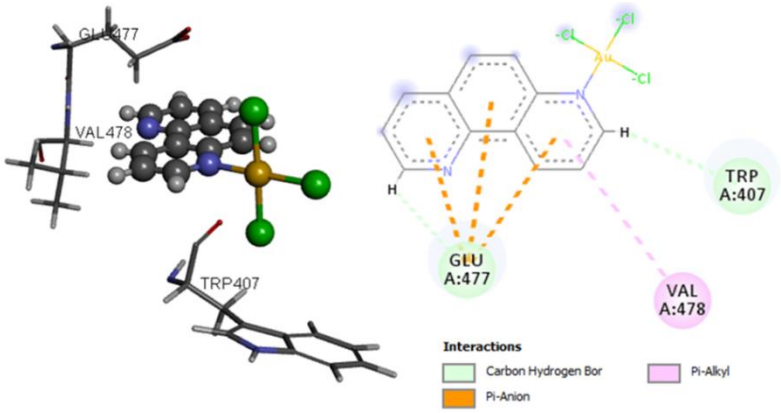
VAL478
TRP407
TRP A:407
GLU A:477
VAL A:478
Interactions
Carbon Hydrogen Bor
Pi-Anion
Pi-Alkyl

1

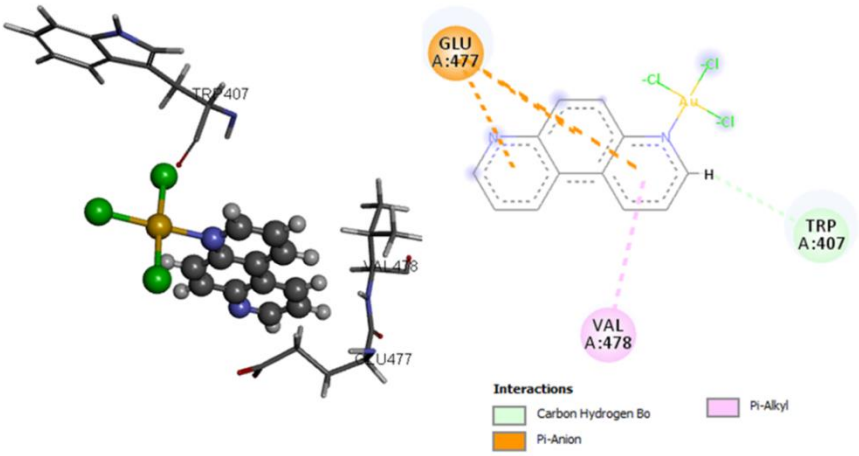
GLU A:477
TRP A:407
VAL A:478
Interactions
Carbon Hydrogen Bo
Pi-Anion
Pi-Alkyl

2

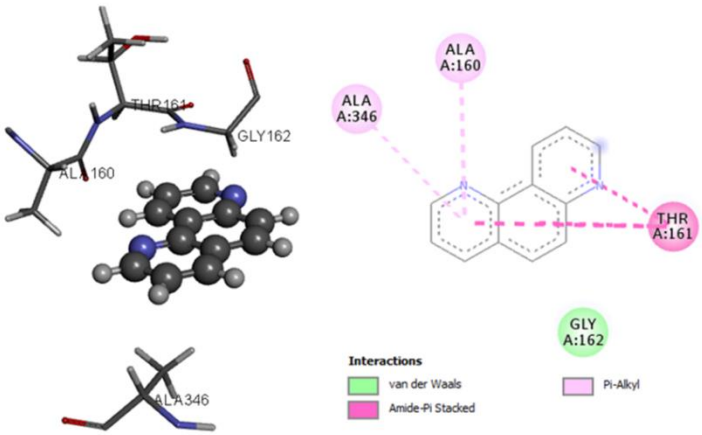
THR161
GLY162
ALA160
ALA346
ALA A:160
ALA A:346
THR A:161
GLY A:162
Interactions
van der Waals
Amide-Pi Stacked
Pi-Alkyl

1,7-phen

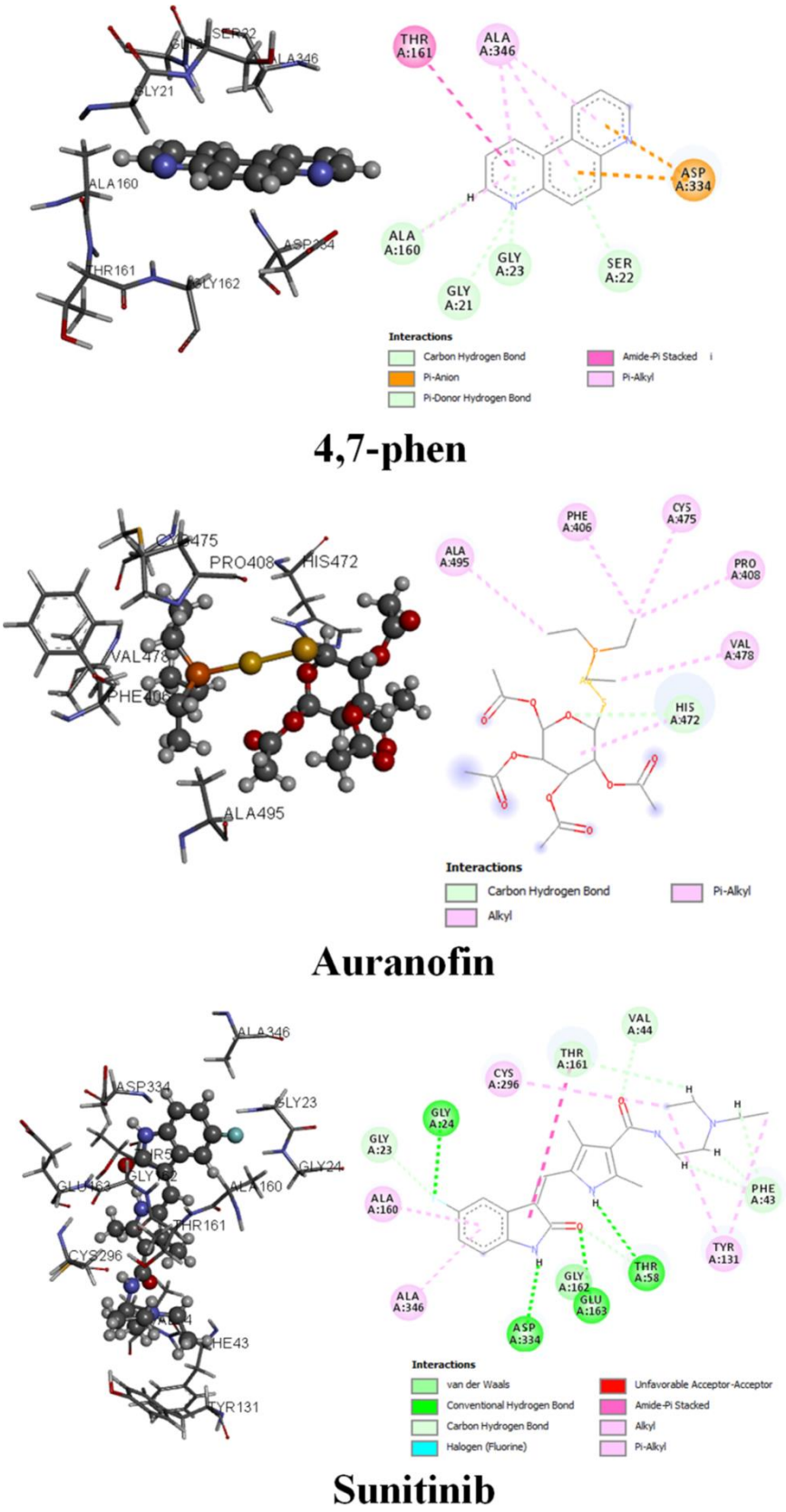

Fig. S16. Interactions of gold(III) complexes **1** and **2**, 1,7- and 4,7-phen, auranofin and sunitinib with selenocysteine residue of TrxR1 protein during molecular docking.

Table S1

Crystal data for **1** and **2**.

For all structures: $C_{12}H_8AuCl_3N_2$, M_r = 483.52. Experiments were carried out at 295 K with Mo *K*α radiation. H-atom parameters were constrained.

	1	**2**
Crystal data		
Crystal system, space group	Monoclinic, $P2_1/c$	Triclinic, $P\bar{1}$
a, *b*, *c* (Å)	12.1848(3), 14.1996(3), 7.7110(2)	7.8420(12), 8.8631(14), 10.7500(5)
α, β, γ (°)	90, 95.833(2), 90	78.707(8), 87.300(8), 66.988(15)
V (Å^3)	1327.24(6)	674.04(17)
Z	4	2
D_x (Mg m^{-3})	2.420	2.382
μ (mm^{-1})	11.67	11.49
Crystal size (mm)	0.18 × 0.05 × 0.03	0.18 × 0.05 × 0.03
Data collection		
Absorption correction	Analytical	Multi-scan
T_{min}, T_{max}	0.093, 0.780	0.903, 1.000
No. of measured, independent and observed [$I > 2\sigma(I)$] reflections	18485, 2336, 2126	4091, 4091, 3247
R_{int}	0.041	
$(\sin\theta/\lambda)_{max}$ (Å^{-1})	0.595	0.596
Refinement		
$R[F^2 > 2\sigma(F^2)]$, $wR(F^2)$, *S*	0.019, 0.044, 1.08	0.036, 0.083, 0.93
No. of reflections	2336	4091
No. of parameters	163	164
$\Delta\rho_{max}$, $\Delta\rho_{min}$ (e Å^{-3})	0.83, -0.56	1.08, -0.87
Percent Filled Space (K.P.I.) (%)[a]	69.2	67.9

[a]For definition see: A.I. Kitajgorodskij, *Molecular Crystals and Molecules*, New-York, Academic Press, 1973.

Table S2

Lethal and teratogenic effects observed in zebrafish (*Danio rerio*) embryos at different hours post fertilization (hpf).

Category	Developmental endpoints	Exposure time (hpf)			
		24	48	72	96/114
Lethal effect	Egg coagulation[a]	●	●	●	●
	No somite formation	●	●	●	●
	Tail not detached	●	●	●	●
	No heartbeat		●	●	●
Teratogenic effect	Malformation of head	●	●	●	●
	Malformation of eyes[b]	●	●	●	●
	Malformation of sacculi/otoliths[c]	●	●	●	●
	Malformation of chorda	●	●	●	●
	Malformation of tail[d]	●	●	●	●
	Scoliosis	●	●	●	●
	Heartbeat frequency		●	●	●
	Blood circulation		●	●	●
	Pericardial edema	●	●	●	●
	Yolk edema	●	●	●	●
	Yolk absosrption	●	●	●	●
	Growth retardation[e]	●	●	●	●

[a]No clear organs structure is recognized.
[b]Malformation of eyes was recorded for the retardation in eye development and abnormality in shape and size.
[c]Presence of no, one or more than two otoliths per sacculus, as well as reduction and enlargement of otoliths and/or sacculi (otic vesicles).
[d]Tail malformation was recorded when the tail was bent, twisted or shorter than to control embryos as assessed by optical comparation.
[e]Growth retardation was recorded by comparing with the control embryos in development or size (before hatching, at 24 and 48 hpf) or in a body length (after hatching, at and onwards 72 hpf) using by optical comparation using an inverted microscope (CKX41; Olympus, Tokyo, Japan).

Table S3

Selected bond distances (Å) and valence angles (°) of the gold(III) complexes **1** and **2**.

	1		**2**	
	X-ray	DFT-calculated	X-ray	DFT-calculated
Au—N[a]	2.049(3)	2.0477	2.066(7)	2.0490
Au—Cl1	2.2858(10)	2.3007	2.284(3)	2.3005
Au—Cl2	2.2643(10)	2.2789	2.273(2)	2.2788
Au—Cl3	2.2701(12)	2.2993	2.273(3)	2.2997
N—Au—Cl1	89.64(9)	89.0716	89.5(2)	89.1026
N—Au—Cl2	178.07(10)	178.6975	179.9(3)	178.4938
N—Au—Cl3	88.90(9)	88.7922	88.9(2)	88.7689
Cl1—Au—Cl2	90.29(4)	91.1128	90.58(11)	91.0814
Cl1—Au—Cl3	178.49(4)	177.8293	176.79(11)	177.8456
Cl2—Au—Cl3	91.16(4)	91.0316	91.04(11)	91.0551
Au—N—C6a	121.0(2)	121.8445		
Au—N—C8	118.4(3)	116.9398		
Au—N—C4a			122.2(6)	122.0368
Au—N—C3			116.1(6)	116.5949

[a]N7 for the complex **1** and N4 for the complex **2**.

Table S4

Geometrical parameters describing intermolecular interactions in the crystals of **1** and **2**[a,b].

	D–H [Å]	D···A [Å]	H···A [Å]	D-H···A [°]	Symmetry operations on A
1					
C2–H2···N1	0.93	3.632(5)	2.79	151	*-x+1,-y+2,-z+1*
C3–H3···Cl1	0.93	3.753(5)	2.87	158	*-x+1,+y+1/2,-z+1/2+1*
C4–H4···Cl3	0.93	3.832(4)	2.92	166	*-x+1,-y+1,-z+1*
C8–H8···Cl1	0.93	3.705(4)	2.87	150	*-x,-y+1,-z+1*
C9–H9···Cl1	0.93	3.600(4)	2.96	127	*x,-y+1/2+1,+z-1/2*
C9–H9···Cl2	0.93	3.701(4)	2.93	141	*-x,+y+1/2,-z+1/2*
2					
C2–H2···N7	0.93	3.398(13)	2.48	171	*x+1,+y-1,+z*
C9–H9···Cl1	0.93	3.713(12)	2.87	151	*-x,-y+1,-z*
C9–H9···Cl3	0.93	3.544(11)	2.88	129	*-x+1,-y+1,-z*
C8–H8···Cl2	0.93	3.820(10)	2.92	164	*x-1,+y+1,+z-1*
C5–H5···Cl3	0.93	3.573(12)	2.84	137	*-x+1,-y+1,-z+1*
C3–H3···Cl1	0.93	3.713(9)	2.83	160	*-x+1,-y,-z+1*
C1–H1···Cl2	0.93	3.778(11)	2.88	163	*x,+y,+z-1*

Cl···Cl Au···Cl	X···X [Å]	d [Å]	θ_1 / θ_2 [°]	type	Symmetry operations
1	Cl1···Cl3	3.4374(16)	149.30(6) / 149.01(7)	I	*x,+y,+z+1*
	Cl1···Au1	3.4074(11)			*-x,-y+1,-z+1*
2	Cl1···Cl3	3.534(4)	150.35(14) / 152.35(15)	I	*x-1,+y,+z*
	Cl1···Au1	3.786(3)			*-x+1,-y,-z+1*

Off-Face stacking	h [Å]	r [Å]	θ [°]	Symmetry operations
1	3.887	0.404	14	*x,-y+1/2+1,+z-1/2*
2	3.486	1.613	0	*-x,-y+1,-z*

[a]For description of parameters describing the halogen bonds see G.R. Desiraju, R. Parthasarathy, J. Am. Chem. Soc. 111 (1989) 8725-8726; A. Mukherjee, S. Tothadi, G.R. Desiraju, Acc. Chem. Res. 47 (2014) 2514-2524.

[b]For description of parameters describing stacking interactions see M. L. Główka, D. Martynowski, K. Kozłowska, J. Mol. Struct. 474 (1999) 81-89.

Table S5

Crucial interatomic distances (Å) in the structures involved in the mechanism of the reaction of $[AuCl_4]^-$ with 1,7- and 4,7-phen calculated at the M06-2X/cc-PVTZ+LanL2TZ(f) level of theory.

	Au1—N7	**Au1—Cl1**	**Au1—Cl2**	**Au1—Cl3**	**Au1—Cl7**	**Au2—N1**	**Au2—Cl4**	**Au2—Cl5**	**Au2—Cl6**	**Au2—Cl8**
RC$^{1,7\text{-phen}}$	2.9590	2.3100	2.3106	2.3088	2.3085	3.2725	2.3063	2.3080	2.3061	2.3055
TS$^{1,7\text{-phen}}$ -1	2.3957	2.3005	2.3278	2.2963	2.6415	3.1989	2.3048	2.3081	2.3067	2.3042
IC$^{1,7\text{-phen}}$	2.0507	2.3053	2.2929	2.3081	3.2298	3.4059	2.3037	2.3048	2.3085	2.3028
TS$^{1,7\text{-phen}}$ -2	2.0549	2.3051	2.2878	2.3082	3.2150	2.4048	2.2980	2.3069	2.2961	2.7140
PC$^{1,7\text{-phen}}$	2.0637	2.3078	2.2862	2.3057	3.1860	2.0838	2.3062	2.2788	2.3079	3.2069
	Au1—N4	**Au1—Cl1**	**Au1—Cl2**	**Au1—Cl3**	**Au1—Cl7**	**Au2—N7**	**Au2—Cl4**	**Au2—Cl5**	**Au2—Cl6**	**Au2—Cl8**
RC$^{4,7\text{-phen}}$	2.9611	2.3111	2.3091	2.3113	2.3088	2.9622	2.3113	2.3091	2.3112	2.3089
TS$^{4,7\text{-phen}}$ -1	2.4037	2.2994	2.3253	2.2955	2.6426	2.9530	2.3097	2.3089	2.3088	2.3084
IC$^{4,7\text{-phen}}$	2.0538	2.3068	2.2884	2.3062	3.2286	2.9503	2.3092	2.3098	2.3084	2.3083
TS$^{4,7\text{-phen}}$ -2	2.0574	2.3057	2.2871	2.3076	3.1974	2.3957	2.2952	2.3173	2.3000	2.6631
PC$^{4,7\text{-phen}}$	2.0628	2.3044	2.2846	2.3079	3.1876	2.0627	2.3046	2.2846	2.3076	3.1877

Table S6

Evaluation of anti-angiogenic potential of gold(III) complexes in comparison to 1,7- and 4,7-phenanthroline, $K[AuCl_4]$ and clinically used drugs auranofin and sunitinib.

Compound	Affected embryos (%)[a]	ISVs (number)			Inhibition (%)	
		Intact	Defective	Absent	ISVs	SIVs
DMF (0.035%)	3.3 ± 0.6	28.4 ± 0.7	0.5 ± 0.7	0.0 ± 0.0	0.3 ± 1.1	0.1 ± 0.03
[$AuCl_3$(1,7-phen-κ*N*7)] (1)						
20 μM	100.0 ± 0.0	0.3 ± 0.5	13.5 ± 1.2	14.2 ± 0.9	77.3 ± 1.1	100 ± 0.0
10 μM	100.0 ± 0.0	5.2 ± 1.1	19.0 ± 1.6	3.8 ± 0.8	51.9 ± 2.7	80.2 ± 0.3
5 μM	63.3 ± 5.1	17.3 ± 0.8	9.0 ± 0.7	1.9 ± 0.6	45.8 ± 3.6	74.2 ± 1.0
2.5 μM	50.0 ± 3.3	20.7 ± 1.3	5.3 ± 1.1	2.1 ± 0.9	39.4 ± 1.9	58.5 ± 1.8
1,7-phen						
20 μM	96.7 ± 4.3	17.7 ± 1.6	8.4 ± 0.8	1.9 ± 1.6	47.8 ± 1.1	55.3 ± 1.9
10 μM	56.7 ± 1.9	20.1 ± 0.9	6.1 ± 01	2.0 ± 0.7	32.8 ± 1.8	44.5 ± 3.0
5 μM	10.0 ± 2.1	25.1 ± 0.7	1.9 ± 0.7	1.0 ± 0.7	25.4 ± 2.0	29.6 ± 3.8
2.5 μM	3.3 ± 0.6	28.0 ± 0.1	0.0 ± 0.0	0.1 ± 0.3	13.1 ± 1.2	13.0 ± 0.6
[$AuCl_3$(4,7-phen-κ*N*4)] (2)						
20 μM	100.0 ± 0.0	9.0 ± 1.1	10.7 ± 1.3	8.3 ± 1.6	64.3 ± 0.8	86.3 ± 0.1
10 μM	90.0 ± 0.0	14.4 ± 1.3	11.5 ± 1.2	2.3 ± 0.8	52.1 ± 0.3	76.8 ± 0.4
5 μM	46.7 ± 2.1	21.2 ± 2.5	7.2 ± 0.8	0.3 ± 0.5	41.3 ± 4.1	49.3 ± 0.1
2.5 μM	20.0 ± 2.7	24.0 ± 0.9	4.1 ± 1.1	0.1 ± 0.3	33.4 ± 1.6	37.4 ± 0.8
4,7-phen						
20 μM	76.7 ± 4.2	15.2 ± 0.6	10.9 ± 0.7	1.9 ± 1.1	32.6 ± 0.8	51.3 ± 0.5
10 μM	43.3 ± 1.7	16.8 ± 1.2	9.1 ± 1.1	2.2 ± 0.8	20.7 ± 2.1	36.6 ± 0.7
5 μM	6.7 ± 1.2	27.5 ± 0.9	0.5 ± 0.2	0.0 ± 0.0	18.2 ± 3.0	33.0 ± 0.1
2.5 μM	0.0 ± 0.0	28.3 ± 0.5	0.0 ± 0.0	0.0 ± 0.0	8.8 ± 0.4	5.8 ± 1.0
$K[AuCl_4]$						
20 μM	30. ± 5.8	25.6 ± 1.1	2.4 ± 1.1	0.0 ± 0.0	6.7 ± 0.6	2.7 ± 0.5
Auranofin						
1.25 μM	100.0 ± 0.0	13.0 ± 1.1	13.6 ± 0.7	1.6 ± 1.1	31.8 ± 1.7	58.0 ± 0.3
Sunitinib						
1.25 μM	100.0 ± 0.0	7.9 ± 1.2	17.7 ±	2.4 ± 0.5	32.9 ± 4.1	59.0 ± 0.4

[a]The percentage of zebrafish embryos displaying anti-angiogenic phenotype.